Available online at www.sciencedirect.com
SCIENCE DIRECT®
Journal of Magnetic Resonance 178 (2006) 65–71
JMR Journal of Magnetic Resonance
www.elsevier.com/locate/jmr

A $^{1}H/^{19}F$ minicoil NMR probe for solid-state NMR: Application to 5-fluoroindoles

Steffen P. Graether [a,1], Jeffrey S. DeVries [a,1], Robert McDonald [b], Melissa L. Rakovszky [a], Brian D. Sykes [a,*]

[a] CIHR Group in Protein Structure and Function, Department of Biochemistry, University of Alberta, Edmonton, Alta., Canada T6G 2H7
[b] X-ray Crystallography Laboratory, Department of Chemistry, University of Alberta, Edmonton, Alta., Canada T6G 2G2

Received 22 June 2005; revised 22 August 2005
Available online 27 September 2005

Abstract

We show that it is feasible to use a minicoil for solid-state ^{19}F ^{1}H NMR experiments that has short pulse widths, good RF homogeneity, and excellent signal-to-noise for small samples while using low power amplifiers typical to liquid-state NMR. The closely spaced resonant frequencies of ^{1}H and ^{19}F and the ubiquitous use of fluorine in modern plastics and electronic components present two major challenges in the design of a high-sensitivity, high-field $^{1}H/^{19}F$ probe. Through the selection of specific components, circuit design, and pulse sequence, we were able to build a probe that has low ^{19}F background and excellent separation of ^{1}H and ^{19}F signals. We determine the principle components of the chemical shift anisotropy tensor of 5-fluoroindole-3-acetic acid (5FIAA) and 5-fluorotryptophan. We also solve the crystal structure of 5FIAA, determine the orientation dependence of the chemical shift of a single crystal of 5FIAA, and predict the ^{19}F chemical shift based on the orientation of the fluorine in the crystal. The results show that this $^{1}H/^{19}F$ probe is suitable for solid-state NMR experiments with low amounts of biological molecules that have been labeled with ^{19}F.
© 2005 Elsevier Inc. All rights reserved.

Keywords: Fluorine; Crystal structure; Minicoil; Probe design; Solid-state

1. Introduction

Biomolecular NMR has always evolved to tackle problems that had been considered "too difficult" by developing new methodologies. Recent examples include TROSY for large proteins [1], cold probes [2,3], and microcoils [4] for low concentration samples, and solid-state NMR for membrane proteins [5,6]. A promising application is the use of ^{19}F as a reporter group in biological molecules. Fluorine NMR has a number of advantages, including a nuclear spin of 1/2, a chemical shift anisotropy (CSA) on the order of at least 100 ppm and high sensitivity due to a high-magnetogyric ratio [7]. ^{19}F is also 100% naturally abundant, and the biological background is minimal since only six distinct natural compounds containing fluorine have been described [8]. The stereochemical similarity of ^{19}F to both H and OH groups allows it to be readily incorporated into amino acids, nucleic acids, and drugs, where fluorine can be used to study their binding properties, structure, and orientation in a magnetic field. For a recent review on the use of fluorine in biomolecular NMR, see Ulrich [9].

There are, however, a number of difficulties in the use of ^{19}F NMR. The γ_F and γ_H differ by ~6%, necessitating the use of elaborate filters and circuit design to prevent radio frequency (RF) resonant signals at one frequency interfering with that at the other in multipulse and broadband decoupling experiments. In a typical ^{19}F NMR experiment, microwatt signals from ^{19}F need to be measured while ^{1}H irradiation is occurring at hundreds of watts. Additionally, the >100 ppm CSA results in rapidly decaying fids and requires the collection of large sweepwidths, which can tax high-field spectrometers. Strong $^{1}H/^{19}F$ and $^{19}F/^{19}F$

* Corresponding author. Fax: +1 780 492 0886.
E-mail address: brian.sykes@ualberta.ca (B.D. Sykes).
[1] These authors contributed equally to this work.

1090-7807/$ - see front matter © 2005 Elsevier Inc. All rights reserved.
doi:10.1016/j.jmr.2005.08.010

dipole–dipole interactions also place demands on the pulse sequences and complicate spectral analysis. Suppression of the $^{1}H/^{19}F$ dipolar interactions is necessary if weak $^{19}F/^{19}F$ dipolar interactions are to be detected. While not abundant in natural compounds, fluorine is ubiquitously used in plastics and especially in materials used in electronic circuits, which results in high-background signal in ^{19}F NMR experiments using commercially available ^{1}H NMR probes. As such, components and materials must be judiciously selected for their use in a ^{19}F NMR probe.

We present here the design and implementation of a $^{1}H/^{19}F$ single input, double-tuned circuit, narrow bore NMR probe using a minicoil for solid-state experiments on biological samples. This probe provides low ^{19}F background, short pulses, good RF homogeneity, and high signal-to-noise (S/N) for small samples using low power amplifiers and components. We also demonstrate the use of an NMR minicoil probe with solid samples, determine the magnitude of the ^{19}F CSA for two fluoroindoles, and determine the orientation of fluorine atoms in a fluoroindole crystal.

2. Coil design

A 1.7-mm capillary design was chosen for the probe coil, since it offers an increased S/N for small samples compared to the 5-mm coils typically used in liquid-state NMR. The coils were constructed from 18 AWG (1.024-mm diameter) oxygen-free copper wire (Fig. 1A) (MWS Wire Industries, Westlake Village, CA). Coils were formed by winding the wire around the sample capillary to ensure a maximum filling factor. The five-turn sample coil measured 6.25-mm long with a 2-mm outer diameter. The sample capillary (melting-point capillary, Kimax–Kontes Vineland, NJ) was chosen with an OD ≅ 1.7 mm. The volume of sample in the capillary was approximately 10 μL. It has been shown that at a fixed length to diameter ratio of a coil, the S/N ratio increases as the diameter is decreased [10]. This is advantageous with biological samples where a limited amount of material may be available. Microcoils have an additional advantage that lower power (or a shorter pulse width at the same power) is required to implement NMR experiments, thereby reducing the potential for arcing in the probe and allowing amplifiers used in liquid-state NMR to be used for solid-state experiments.

3. Probe and circuit components

One important aspect in the selection of electronic components is that they do not contain fluorine, which is often present in the component's insulation, grease, and dielectrics. The presence of polytetrafluoroethylene (PTFE) in the trimmer capacitors used in this probe required a compromise to be made; the lengths of the leads of the sample coil in the circuit needed to be long enough so that the PTFE dielectric is outside the effective B_1 field (to keep background low), yet short enough so as not to increase unwanted stray inductance and capacitance in the circuit. The result is a distance of 5 cm between the tops of the capacitors and the bottom of the ^{19}F minicoil. The remaining background was reduced by the use of the DEPTH pulse sequence [11], which selects for homogeneous regions of the RF field.

4. Probe design

The probe body was constructed from a 600 MHz Varian triple-resonance liquid-state probe with a 38-mm outer

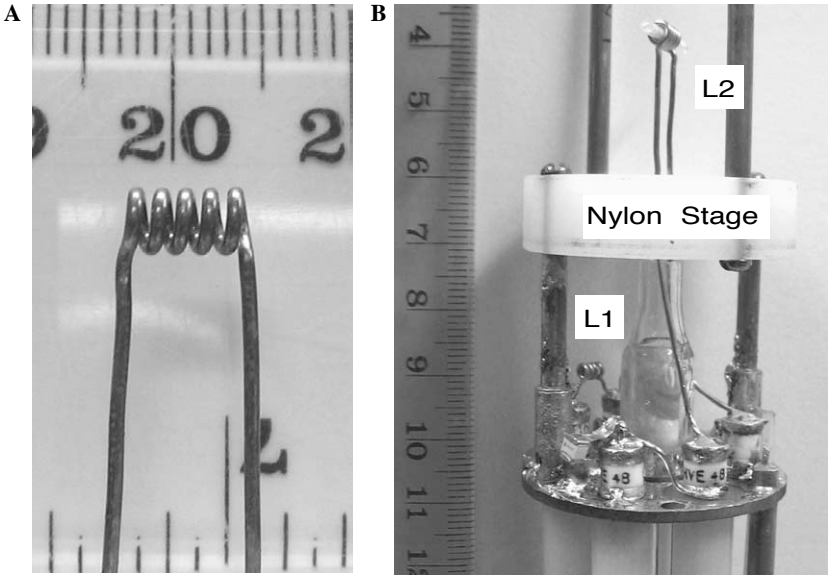

Fig. 1. (A) View of the sample minicoil. (B) Circuit design and layout showing a view of the components within the probe. All ruler divisions are in millimeter.

diameter. The inside of the probe head consists of three segments (Fig. 1B). The bottom segment was constructed from a grounded printed circuit board (PCB), on which the trimmer and chip capacitors and the coupling coil were soldered. The middle segment consists of a 10-mm thick piece of nylon to stabilize the sample coil from external mechanical vibrations. The top segment contains the sample coil. A 10-mm thick brass plate was inserted in the probe head cover, which provides a grounding shield from external resonant frequencies above the sample coil. A 5-mm opening in the center of each segment allows for variable temperature airflow. A semi-rigid, coax cable with PTFE dielectric was used for the transmit and receive paths between the probe circuit and probe port because of its higher power handling capabilities.

In addition to low fluorine content, capacitors were chosen so as to be non-magnetic, small in size, capable of high-working voltages, and have low capacitance (picofarad range). NMKT10HVE (1000 WVDC, Voltronics, Denville, NJ) trimmer capacitors were chosen for this application. The chip capacitors chosen were 500 WVDC with a capacitance of 7.5 pF (100B7R5CMS) and 36 pF (100B360GMS500) from American Technical Ceramic (Huntington Station, NY).

5. Circuit design

To allow for separation of the closely spaced $^{1}H/^{19}F$ resonances in high-power experiments, a series resonant, capacitor-coupled, band pass filter circuit was chosen (Fig. 2A). The basic circuit design consists of two resonant circuits of L1 and C2, and C4, C5, and L2, where L1 designates the coupling coil, L2 designates the sample coil, and C designates the capacitors. The two circuits are coupled together via capacitors C3a and C3b. C3a is a trimmer capacitor that is adjusted so as to create an over-coupled condition, resulting in a single port, double-tuned circuit [12]. A second set of capacitors (C1a and C1b) was placed at the beginning of the circuit in a parallel configuration to provide proper impedence matching to a 50 Ω input. C1a is a trimmer capacitor that allows for fine tuning of the matching condition. The sample coil is balanced by placing trimmer capacitors C4 and C5 on both ends in a series configuration (R. Chang and W. Brey, personal communication). These trimmer capacitors were adjusted until a uniform B_1 field was achieved (R. Chang and W. Brey, personal communication). The signal from the single port is split into two channels using a directional coupler with ^{1}H and ^{19}F bandpass filters (DP564-600-5BB, Spectrum

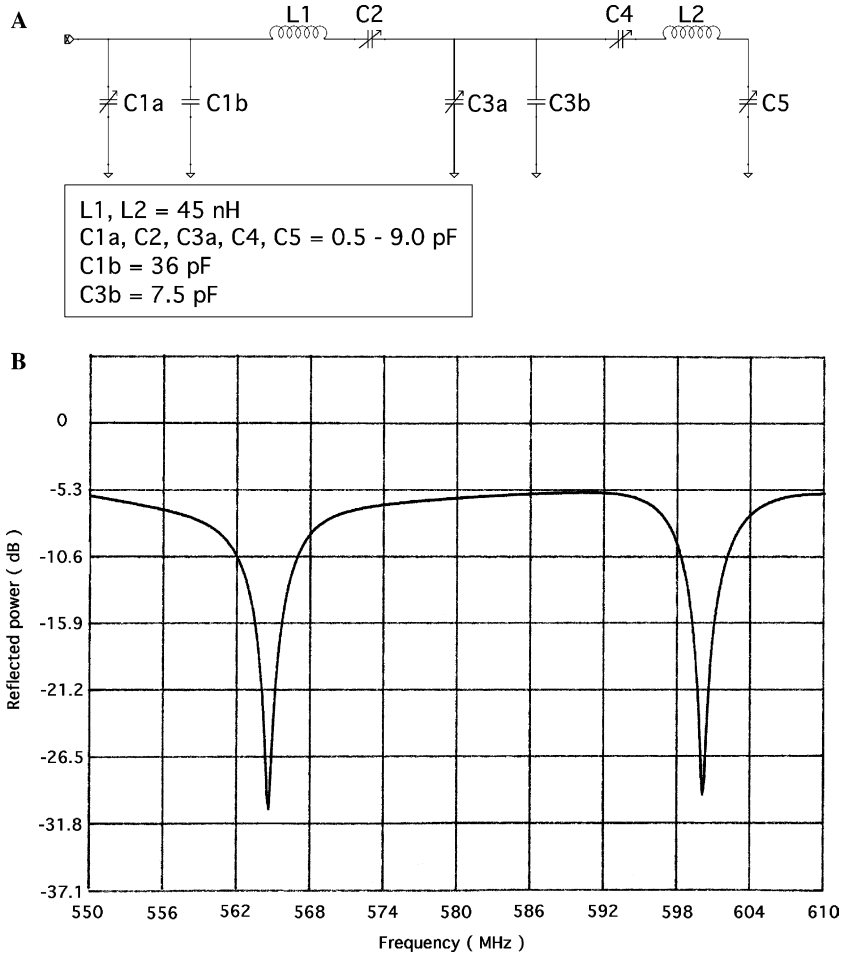

Fig. 2. (A) Circuit schematic. The physical series resonant, capacitor-coupled band pass filter used in the probe. The component labels are described in the main text. (B) Double-resonance tuning and matching at the ^{19}F resonant frequency.

FSY Microwave, Palm Bay, FL), which separates the ^{1}H and ^{19}F signals before transmission to the spectrometer.

6. Results and discussion

The tuning, matching, and over-coupling capabilities of the probe circuit were observed on an Oxford 14.09 T magnet using a Varian INOVA^{UNITY} spectrometer (Fig. 2B). Final tuning and matching of the probe was made by adjusting the C2 (^{1}H) and C4 (^{19}F) capacitors using the Varian QTUNE software. Table 1 contains Q values that were measured from a graph of reflected power versus frequency (Fig. 2B) as follows:

$$Q = \frac{f_0}{f_1[-3\ \mathrm{dB}] - f_2[-3\ \mathrm{dB}]}, \quad (1)$$

where f_0 is the resonant frequency of the respective channel, and f_1 and f_2 are the frequencies at -3 dB from the baseline of total reflection of the respective resonant frequency, which is defined as bandwidth. Fig. 2B shows that a good separation of the two resonant frequencies has been achieved. The circuit efficiency and coil homogeneity were tested by using a 10 μL liquid standard sample of 0.1 M trifluoroacetic acid (TFA) in 90% H_2O/10% D_2O at 21 °C. Typical, but not maximum power, 90° pulse width and γB_1 are summarized in Table 2. A γB_1 of 100 kHz is easily obtained with only 12.5 W of transmitted power for ^{19}F observe, demonstrating that kilowatt power amplifiers are not required for this probe. The linewidth at half-height was 200 Hz at 600 MHz. RF homogeneity is 94% for this probe (defined as the ratio of the peak height at a 450° tip angle over the peak height at a 90° tip angle multiplied by 100).

To test the suitability of the probe for biological experiments, solid-state NMR experiments were performed using 5-fluoroindole-3-acetic acid (5FIAA, Fig. 3A). The crystallization conditions and structure of 5FIAA have already been determined [13], making 5FIAA suitable for the single-crystal experiments described below. First, we collected the powder pattern spectrum of 3.3 mg 5FIAA to determine the principal values of the CSA tensor

Table 1
Probe Q value

Nucleus	Frequency (MHz)	Reflected power (dB)	Q value
^{19}F	564.355	−29.6	122
^{1}H	599.858	−28.5	124

Table 2
Typical probe operating characteristics

Nucleus	Power (W)	pw90 (μs)	γB_1 (kHz)
^{19}F	12.5	2.50	100
	16	2.15	116
	25	2.00	125
	32	1.65	152
^{1}H	16	3.50	71

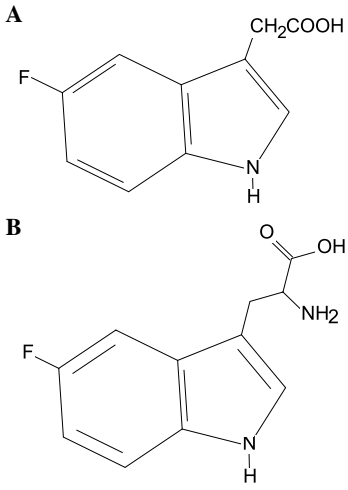

Fig. 3. (A) Structure of 5-fluoroindole-3-acetic acid. (B) Structure of 5-fluorotryptophan.

(Fig. 4A, top). The values of 5FIAA were determined to be $\delta_{11} = -0.8$, $\delta_{22} = -71.7$, and $\delta_{33} = -78.7$ ppm relative to TFA at 0 ppm, where TFA is at −76.53 ppm relative to $CFCl_3$ at 0 ppm. There is a notable inflection in the spectrum at −12.8 ppm, which results from the homonuclear $^{19}F/^{19}F$ dipolar splitting corresponding to closely spaced ^{19}F nuclei in the crystalline powder (see structure below). A simulation of the powder pattern using SIMPSON [14] was used to investigate this interaction (Fig. 4A, bottom). For the simulation of the 5FIAA powder pattern, we used the zcw28656 crystal file, which describes 28,656 random orientations in a powder. Using the principal values above, we obtain a δ_{iso} of −50.4 ppm, a δ_{aniso} of 49.6 and a η of 0.14. For the purpose of simplification we assume that there is one $^{19}F/^{19}F$ dipole interaction between fluorines in the crystal that is co-planar with the C–F bond. We use a $^{19}F/^{19}F$ dipolar coupling of 4000 Hz, which corresponds to a distance of 3.0 Å between the two atoms. This represents a simplification, since there are many fluorine–fluorine interactions in the crystal lattice (see below). Nonetheless, the simulation does represent a reasonable approximation of the experimental data, supporting the conclusion that dipolar interactions are the cause of the inflection point in the powder spectrum of 5FIAA.

A powder pattern of a 4.2 mg sample of 5F-Trp (Fig. 3B) taken under the same conditions as for 5FIAA is shown in Fig. 4B, top. The principal values of the CSA tensor of 5F-Trp were determined to be $\delta_{11} = 2.3$, $\delta_{22} = -71.0$, and $\delta_{33} = -79.7$ ppm relative to TFA at 0 ppm. These values agree well with those determined by ^{19}F MAS NMR with values of $\delta_{11} = 2.6$, $\delta_{22} = -73.6$, and $\delta_{33} = -78.9$ ppm (P. Hazendonk, personal communication). A SIMPSON simulation of 5F-Trp was run under the same conditions as above but without a dipole–dipole interaction (Fig. 4B, bottom). Using our principal values above, we obtain a δ_{iso} of −49.4 ppm, a δ_{aniso} of 51.7 and a η of 0.176. There is some disagreement between these data and those obtained by Grage et al. [15], whose values,

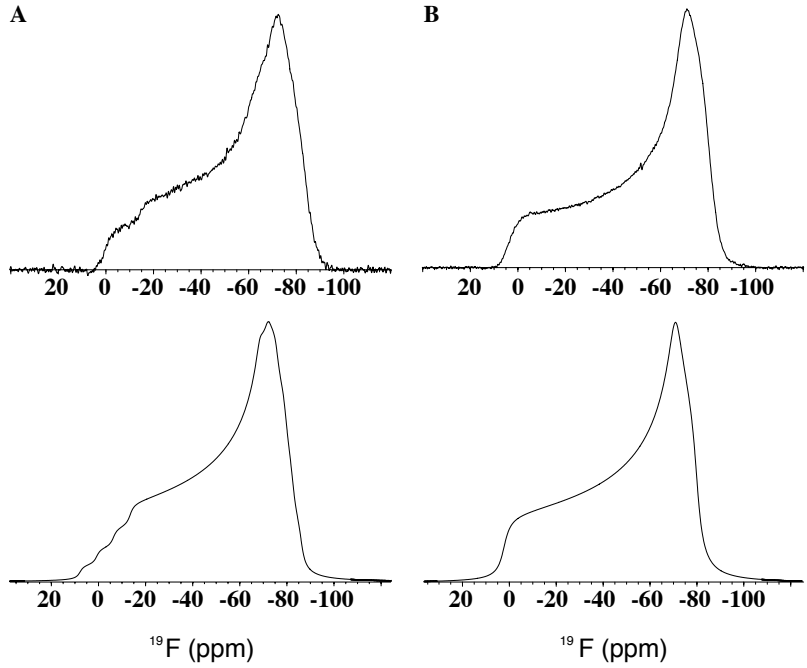

Fig. 4. Powder pattern of two fluoroindoles. (A) Top, 5FIAA ^{19}F powder pattern, using a 90° pulsewidth of 2.0 μs, a recycle time of 200 s, and 352 transients. Bottom, a simulation of the powder pattern using SIMPSON [14]. See the text for details. (B) Top, 5F-Trp ^{19}F powder pattern, using a 90° pulsewidth of 2.1 μs, a recycle time of 150 s, and 384 transients. Bottom, a SIMPSON simulation of the powder pattern. All experiments were collected with the DEPTH pulse sequence using a sweepwidth of 200,000 Hz and ^{1}H decoupling at $\gamma B_1 = 50$ kHz. ^{1}H decoupling did not reduce S/N of the ^{19}F signal.

after shifting δ_{iso} to −50.0 ppm, were $\delta_{11} = -4.0$, $\delta_{22} = -65.5$, and $\delta_{33} = -80.5$ ppm. These differences may reflect the fact that the 5F-Trp was in a lipid environment or the mobility of the sidechains in the Grage et al. experiments.

One use of fluorine labeled biological molecules in oriented samples is to correlate the chemical shift of ^{19}F in the molecule with the orientation of the fluorine atom relative to the magnetic field [9]. To demonstrate the feasibility of this approach, we produced a single crystal of 5FIAA. Because the crystal was grown from a solvent mixture different from that of the solved structure (3:2 methanol/water vs. 1:1:1 propan-2-ol/methanol/water [13]), we collected several frames in order to index the unit cell. The result was different from the previous crystal structure, requiring the complete determination of the structure of 5FIAA in our crystal (Fig. 5A). The molecules of this hydrogen-bonded dimer are crystallographically independent, i.e., they are not related by translational, rotational, or inversion symmetry, whereas in the previously reported structure, carboxylic acid dimers were formed by molecules related by crystallographic inversion centers [13]. The packing of fluorine atoms in the crystal lattice is shown in Fig. 5B. The stacked rings result in the two crystallographically independent molecules having two neighboring fluorines at 4.4 Å. The other neighboring fluorine atoms differ between the two molecules, in one case the neighbor is 3.5 and 3.8 Å away, and in the other both fluorines are 5.1 Å away.

The faces of the pale yellow crystal (dimensions of $0.9 \times 0.3 \times 0.3$ mm^3) were indexed to provide an orientation of the unit cell in the laboratory frame (Fig. 6). The crystal was manually rotated in the minicoil from 0° to 160° (Fig. 7A). The starting angle (0°) is defined as the $\bar{1}01$ plane of the crystal being oriented perpendicular to B_0, though subsequent data analysis found this to be off by −20° due to imperfections on the $10\bar{1}$ face and inaccuracies in the starting orientation in the capillary. Two sets of peaks are observed, one that may be an overlapped doublet, the other which varies between a broad doublet and a broad triplet. Lineshapes are Gaussian, which comes from the dipolar coupling between the multiple fluorine atoms in the crystal [16]. Simulations of the crystal structure show that the difference in the splitting patterns of the peaks can be explained by the ^{19}F/^{19}F dipolar coupling interactions for the two crystallographically independent molecules (Alexander Nevzorov, personal communication).

Based on the determined crystal structure and the relationship:

$$\omega_{CSA} = \omega_0(\delta_{11}\sin^2\theta\cos^2\phi + \delta_{22}\sin^2\theta\sin^2\phi + \delta_{33}\cos^2\theta), \quad (2)$$

where ω_0 is the Larmor frequency, δ_{aa} is the relevant principal value of the CSA tensor, and θ and ϕ are the polar angles that describe the orientation of the CSA tensor relative to B_0, we can calculate the chemical shift at each orientation and compare them to the observed values. The results demonstrate that we are able to predict the chemical

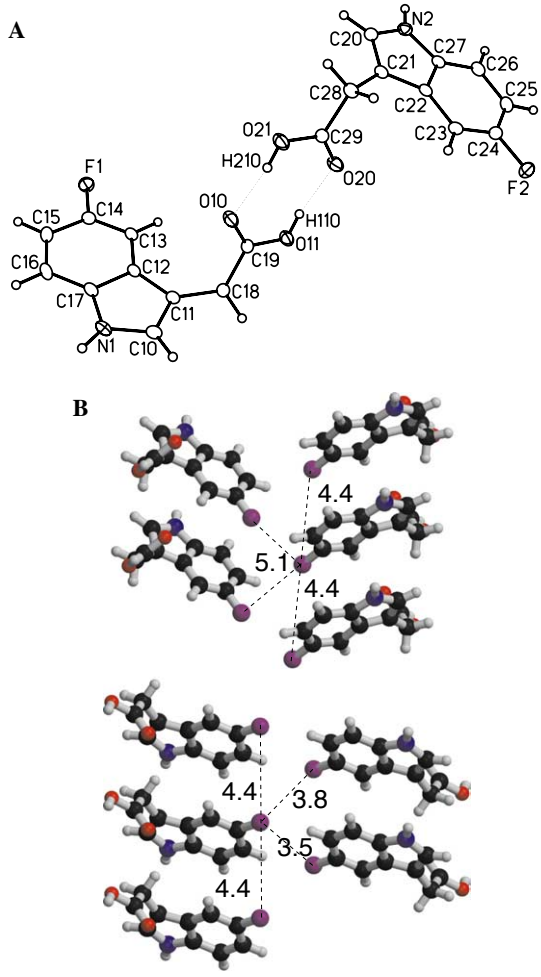

Fig. 5. Crystal structure of 5FIAA. (A) Perspective view showing the mode of crystallization of 5FIAA in this particular polymorph. Non-hydrogen atoms are represented by Gaussian ellipsoids at the 20% probability level. Hydrogen atoms are shown with arbitrarily small thermal parameters. (B) Packing of fluorines in the unit cell. Distances between fluorine atoms less than 6 Å are shown in the figure, with the two crystallographically independent molecules shown separately.

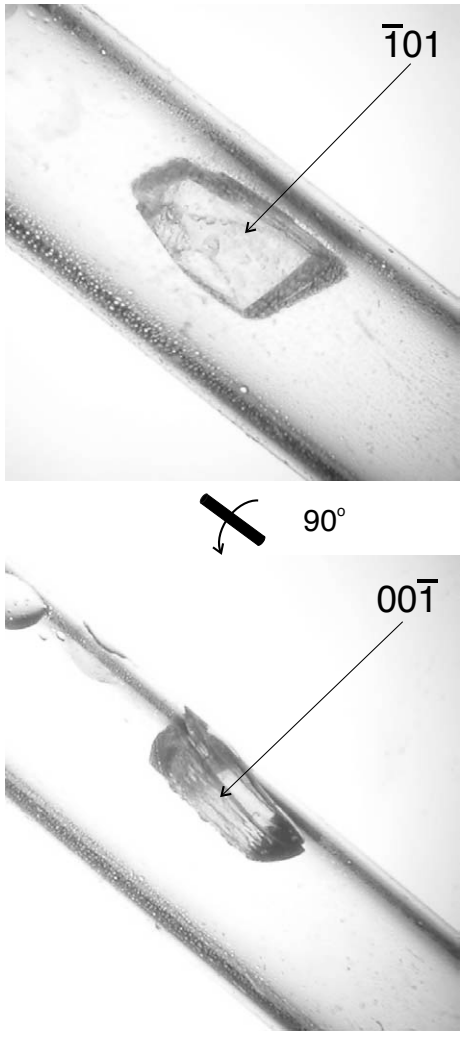

Fig. 6. Crystal habit and faces. The crystal used in the NMR experiments was first indexed by X-ray crystallography to determine the unit cell orientation in the laboratory frame.

shift of the fluorine atom from its orientation in the laboratory frame (Fig. 7B).

7. Experimental

The Q value was measured by sweeping frequencies from 550 to 610 MHz using an Agilent 83752A 0.01–20 GHz synthesized sweep generator while a Hewlett–Packard 87557 scalar network analyzer displayed the reflected power from a Mini Circuits ZF-DC-10-2 directional coupler connected to the probe.

5-Fluoroindole-3-acetic acid (5FIAA, Product F4506, Molecular Formula $C_{10}H_8FNO_2$, Formula Weight 193.17, CAS Number 443-73-2) and 5-fluorotryptophan (5F-Trp, Product F0896, Molecular Formula $C_{11}H_{11}FN_2O_2$, Formula Weight 222.2, CAS Number 154-08-05) were purchased from Sigma–Aldrich Canada (Oakville, ON). Samples were sealed in the capillary using the Triad gel (Dentsply International, York, PA), a non-fluorine liquid sealant that was polymerized using UV light from an Optilux 501 UV source (Kerr Dentistry, Orange CA).

Crystals of 5FIAA were grown after approximately 1 month at room temperature by evaporation from a 12.5 mg/mL solution of 3:2 methanol/water. Crystal data for 5FIAA: crystal system: monoclinic, space group: $P2_1/n$ (an alternate setting of $P2_1/c$ [No. 14]) with unit cell dimensions $a = 17.6080$ (14) Å, $b = 4.4529$ (3) Å, $c = 23.7724$ (18) Å, $\beta = 110.8980$ (11)°, $V = 1741.3$ (2) Å^3, $Z = 8$, $\rho_{calcd} = 1.474$ g cm^{-3}, $\mu = 0.118$ mm^{-1}. A crystal fragment of approximate dimensions of $0.50 \times 0.32 \times 0.26$ mm^3 was mounted in a non-specific orientation on a Bruker SMART 1000 CCD PLATFORM diffractometer system. All intensity measurements were performed using Mo Kα radiation ($\lambda = 0.71073$ Å) with a graphite crystal incident beam monochromator. The intensity data were collected at −80° using ω scans (0.3° scans, 15 s exposures). A total of 3587 independent reflections were collected to a maximum 2θ limit at 52.84°. The structure was solved by direct methods (*SHEL-*

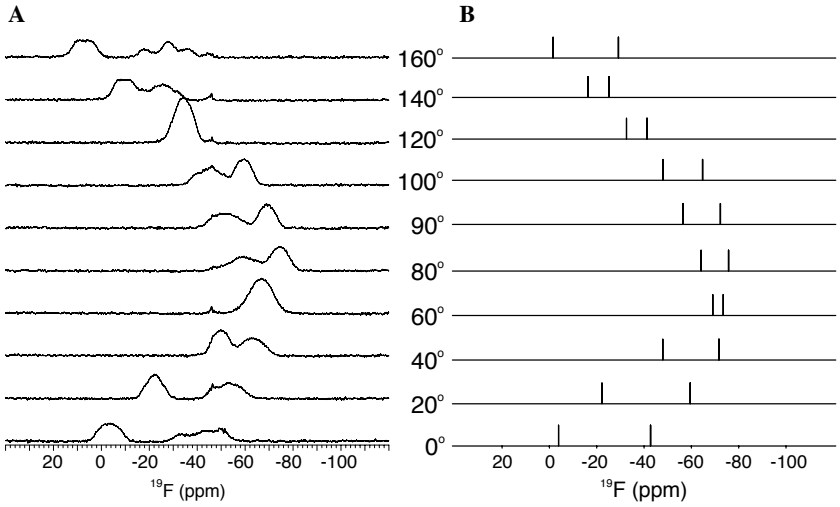

Fig. 7. Rotation of a single crystal in the minicoil. (A) The crystal was rotated by 10° or 20° increments after each DEPTH experiment (32 transients with a 2.1 μs 90° pulse width and 500 s recycle delay). All experiments were collected with the DEPTH pulse sequence using a sweepwidth of 200,000 Hz and ^{1}H decoupling at $\gamma B_1 = 50$ kHz. (B) Prediction of the chemical shift based on the orientation of the unit cell after each rotation.

XS-86). Refinement of atomic parameters was carried out by using full-matrix least-squares on F^2 (*SHELXL-93*), giving final agreement factors (R indices) of $R_1(F) = 0.0354$ (for 3008 data with $I \geqslant 2\ \sigma(I)$) and $wR_2(F^2) = 0.0997$ (for all 3587 unique data). Crystallographic data (excluding structure factors) have been deposited at the Cambridge Crystallographic Data Centre as supplementary publication number CCDC 275074. Copies of the data can be obtained free of charge by application to CCDC, 12 Union Road, Cambridge CB2 1EZ, UK (Fax: +44 1223 336033 or, e-mail: deposit@ccdc.cam.ac.uk or, http://www.ccdc.cam.uk).

Acknowledgments

We thank Drs. Christopher Grant and Chin (Albert) Wu at the University of California (San Diego) for suggestions regarding probe and experimental design; we also thank Dr. Alexander Nevzorov at the University of California (San Diego) for running simulations on the single-crystal data and Dr. Jan Rainey at the University of Alberta for help running the SIMPSON simulations on the powder data. Dr. William Brey and Ran K. Chang at the National High Magnetic Field Laboratory (Florida State University) are thanked for providing information on the design and testing of an over-coupled circuit in an NMR probe. We thank Dr. Paul Hazendonk at the University of Lethbridge for providing the principle components of the chemical shift tensor of 5F-Trp from ^{19}F MAS NMR experiments. Sam Graziano at the University of Alberta is thanked for construction of probe body parts. Dr. Barry Hoffman is thanked for providing Triad gel and an Optilux 501 UV source.

References

[1] K. Pervushin, R. Riek, G. Wider, K. Wuthrich, Attenuated T-2 relaxation by mutual cancellation of dipole–dipole coupling and chemical shift anisotropy indicates an avenue to NMR structures of very large biological macromolecules in solution, Proc. Natl. Acad. Sci. USA 94 (1997) 12366–12371.

[2] P. Styles, N.F. Soffe, C.A. Scott, D.A. Cragg, F. Row, D.J. White, P.C.J. White, A high-resolution Nmr probe in which the coil and preamplifier are cooled with liquid-helium, J. Magn. Reson. 60 (1984) 397–404.

[3] P. Styles, N.F. Soffe, C.A. Scott, An improved cryogenically cooled probe for high-resolution Nmr, J. Magn. Reson. 84 (1989) 376–378.

[4] D.L. Olson, T.L. Peck, A.G. Webb, R.L. Magin, J.V. Sweedler, High-resolution microcoil H-1-Nmr for mass-limited, nanoliter-volume samples, Science 270 (1995) 1967–1970.

[5] S.J. Opella, F.M. Marassi, Structure determination of membrane proteins by NMR spectroscopy, Chem. Rev. 104 (2004) 3587–3606.

[6] A. Watts, S.K. Straus, S.L. Grage, M. Kamihira, Y.H. Lam, X. Zhao, Membrane protein structure determination using solid-state NMR, Methods Mol. Biol. 278 (2004) 403–473.

[7] W.E. Hull, B.D. Sykes, Fluorotyrosine alkaline-phosphatase—internal mobility of individual tyrosines and role of chemical-shift anisotropy As A F-19 nuclear spin relaxation mechanism in proteins, J. Mol. Biol. 98 (1975) 121–153.

[8] D. O'Hagan, D.B. Harper, Fluorine-containing natural products, J. Fluor. Chem. 100 (1999) 127–133.

[9] A.S. Ulrich, Solid state 19F NMR methods for studying biomembranes, Prog. Nucl. Magn. Reson. Spectrosc. 46 (2005) 1–21.

[10] T.L Peck, R.L. Magin, P.C. Lauterbur, Design and analysis of microcoils for Nmr microscopy, J. Magn. Reson. B 108 (1995) 114–124.

[11] D.G. Cory, W.M. Ritchey, Suppression of signals from the probe in bloch decay spectra, J. Magn. Reson. 80 (1988) 128–132.

[12] S.L. Hu, J.A. Reimer, A.T. Bell, Single-input double-tuned circuit for double resonance nuclear magnetic resonance experiments, Rev. Sci. Instrum. 69 (1998) 477–478.

[13] S. Antolic, B. KojicProdic, S. Tomic, B. Nigovic, V. Magnus, J.D. Cohen, Structural studies on monofluorinated derivatives of the phytohormone indole-3-acetic acid (auxin), Acta Crystallogr. B 52 (1996) 651–661.

[14] T. Vosegaard, A. Malmendal, N.C. Nielsen, The flexibility of SIMPSON and SIMMOL for numerical simulations in solid- and liquid-state NMR spectroscopy, Monatshefte Chem. 133 (2002) 1555–1574.

[15] S.L. Grage, J.F. Wang, T.A. Cross, A.S. Ulrich, Solid-state F-19-NMR analysis of F-19-labeled tryptophan in gramicidin A in oriented membranes, Biophys. J. 83 (2002) 3336–3350.

[16] A. Abragam, Principles of Nuclear Magnetism, Clarendon Press, Oxford, UK, 1961.